Supporting Information

Broken-gap type-III band alignment in monolayer halide perovskites/antiperovskite oxides van der Waals heterojunctions

Hongxia Zhong,[a] Zhengyu Xu,[a] Chunbao Feng,[b] Xiaoying Wan,[a] Jiahui Li,[a] Hai Wang[a] and Gang Tang[c†]

[a] *School of Mathematics and Physics, China University of Geosciences (Wuhan), Wuhan, China, 430074.*
[b] *School of Science, Chongqing University of Posts and Telecommunications, Chongqing, China, 400065.*
[c] *Advanced Research Institute of Multidisciplinary Science, Beijing Institute of Technology, Beijing, China, 100081.*

Table S1 The lattice constants for perovskite and antiperovskite.

Compound	**S.G.**	a_{exp} (Å)	b_{exp} (Å)	c_{exp} (Å)	a_{cal} (Å)	
Cs_2CdCl_4	*I4/mmm*	5.260	5.260	16.880	5.351	Ref.[1]
Rb_2CdCl_4	*I4/mmm*	5.207	5.207	16.169	5.279	Ref.[2]
$Rb_2CdCl_2I_2$	*I4/mmm*	5.285	5.285	17.606	5.431	Ref.[3]
$Cs_2PbCl_2I_2$	*I4/mmm*	5.639	5.638	18.879	5.711	Ref.[4]
$Cs_2SnCl_2I_2$	*I4/mmm*	5.591	5.591	18.898	5.631	Ref.[5]
Ba_2ZrS_4	*I4/mmm*	4.715	4.715	16.023	4.931	Ref.[6]
Ba_2HfS_4	*I4/mmm*	4.834	4.834	15.842	4.902	Ref.[6]
Ba_4OSb_2	*I4/mmm*	5.120	5.120	17.950	5.255	Ref.[7]
Ba_4OAs_2	*I4/mmm*	5.125	5.125	17.336	5.128	Ref.[8]
Sr_4OAs_2	*I4/mmm*	4.831	4.831	16.364	4.794	Ref.[8]
Sr_4OP_2	*I4/mmm*	4.794	4.794	15.985	4.736	Ref.[8]
Ca_4OBi_2	*I4/mmm*	4.719	4.719	16.505	4.719	Ref.[9]
Ca_4OSb_2	*I4/mmm*	4.677	4.677	16.342	4.652	Ref.[7]
Ca_4OAs_2	*I4/mmm*	4.537	4.537	15.449	4.487	Ref.[10]
Ca_4OP_2	*I4/mmm*	4.492	4.492	15.087	4.424	Ref.[10]

Considering that two-dimensional (2D) $Cs_2Pb(SCN)_2Br_2$ has been synthesized and successfully used as an absorber for solar cells, we take $Cs_2Pb(SCN)_2Br_2$ as an example to analyze the effects of different calculation method on the band edge positions, which can be compared with the measured results in Fig. S1. PBE calculation without SOC raises the VBM by 0.881 eV and lowers the CBM by 0.220 eV with respect to PBE+SOC, resulting in a band gap of 2.329 eV. Therefore, the SOC effects are important for our studied perovskites containing heavy elements, such as Bi, Sb, Zr, and Hf. Because the PBE usually underestimates the band gaps of semiconductors, we also adopt the HSE06+SOC functional to examine the band edges of 2D $Cs_2Pb(SCN)_2Br_2$. It is shown that the HSE06+SOC method lowers (raises) the VBM (CBM) to -6.039 (-3.575) eV, matching well with the measured band edge positions, eg, VBM of -5.861 eV and CBM of -3.211 eV in experiment[11]. Therefore, we use the HSE06+SOC method for the band edge alignment of all studied perovskites in the whole main text.

According to Table S2, fortunately, compared to the halide perovskites Cs_2CdCl_4 and Rb_2CdCl_4, the antiperovskite oxides Ba_4OSb_2, and Ca_4OBi_2 possess higher VBM and lower CBM, which may lead to type-II band alignment between these perovskites and antiperovskites. For sulfide perovskites Ba_2ZrS_4 and Ba_2HfS_4, their lattice (4.902-4.931 Å) matches the

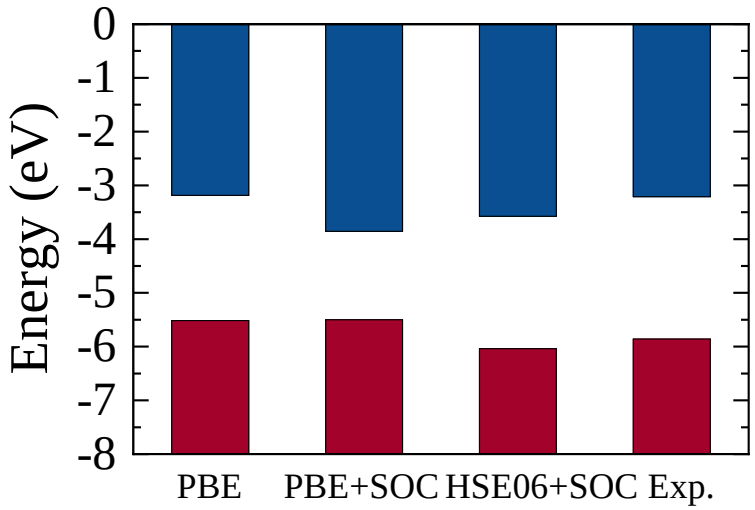

Figure S1 Band alignment for 2D $Cs_2Pb(SCN)_2Br_2$ using PBE, PBE +SOC, and HSE06 + SOC. The experimental band edge is listed for comparison[11].

Table S2 Band gaps and band edges of monolayer perovskite and antiperovskite calculated by HSE06+SOC method. The data obtained by PBE+SOC is also listed. Band edges were aligned by referring the common average potentials.

	HSE+SOC			PBE+SOC		
Compound	Band gap (eV)	VBM (eV)	CBM (eV)	Band gap (eV)	VBM (eV)	CBM (eV)
Cs_2CdCl_4	4.531	-6.580	-2.049	3.250	-5.726	-2.476
Rb_2CdCl_4	4.552	-6.764	-2.212	3.260	-5.913	-2.653
$Rb_2CdCl_2I_2$	3.356	-6.402	-3.046	2.360	-5.714	-3.354
$Cs_2PbCl_2I_2$	2.374	-5.894	-3.520	1.818	-5.320	-3.501
$Cs_2SnCl_2I_2$	1.995	-5.122	-3.127	1.645	-4.729	-3.084
Ba_2ZrS_4	1.294	-5.334	-4.040	0.533	-4.458	-3.925
Ba_2HfS_4	1.483	-4.895	-3.412	0.747	-4.407	-3.660
Ba_4OSb_2	1.067	-3.169	-2.102	0.492	-2.601	-2.109
Ba_4OAs_2	1.348	-3.009	-1.662	0.761	-2.485	-1.724
Sr_4OAs_2	1.594	-3.626	-2.032	0.952	-2.825	-1.874
Sr_4OP_2	1.749	-3.420	-1.671	1.138	-2.814	-1.676
Ca_4OBi_2	1.042	-3.249	-2.207	0.384	-2.948	-2.565
Ca_4OSb_2	1.580	-4.042	-2.462	0.812	-3.308	-2.496
Ca_4OAs_2	1.987	-3.963	-1.976	1.243	-3.166	-1.923
Ca_4OP_2	2.185	-4.070	-1.885	1.416	-3.169	-1.753

range of antiperovsktie oxides well, and their CBM is lower than antiperovskites, thus, also lead to type-III heterostructure with antiperovskite. Moreover, owing to the higher VBM in antiperovskite oxides X_4OA_2, monolayers X_4OA_2 are easily doped *p*-type[12], and difficult to find suitable hole transport layer (HTL)[13], and unfavorable for water splitting. It is noted that for realistic applications, the environment effects are important for these monolayer systems, our calculation of isolated monolayers still serves as a valuable foundation for such studies.

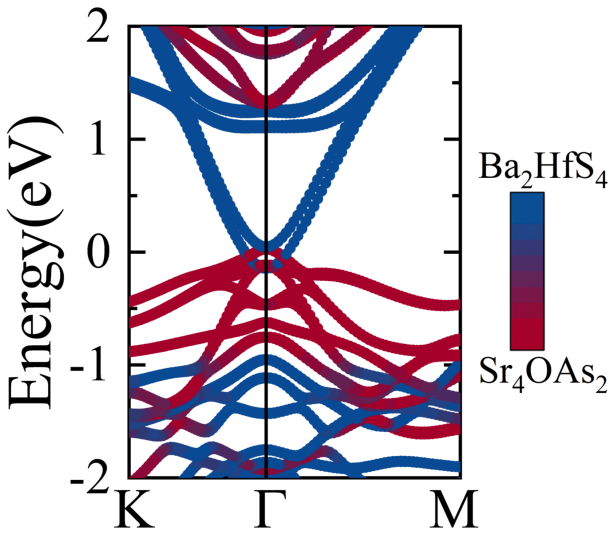

Figure S2 Projected band structure of Ba_2HfS_4/Sr_4OAs_2 heterostructure, clearly demonstrating the typical type-III characteristic.

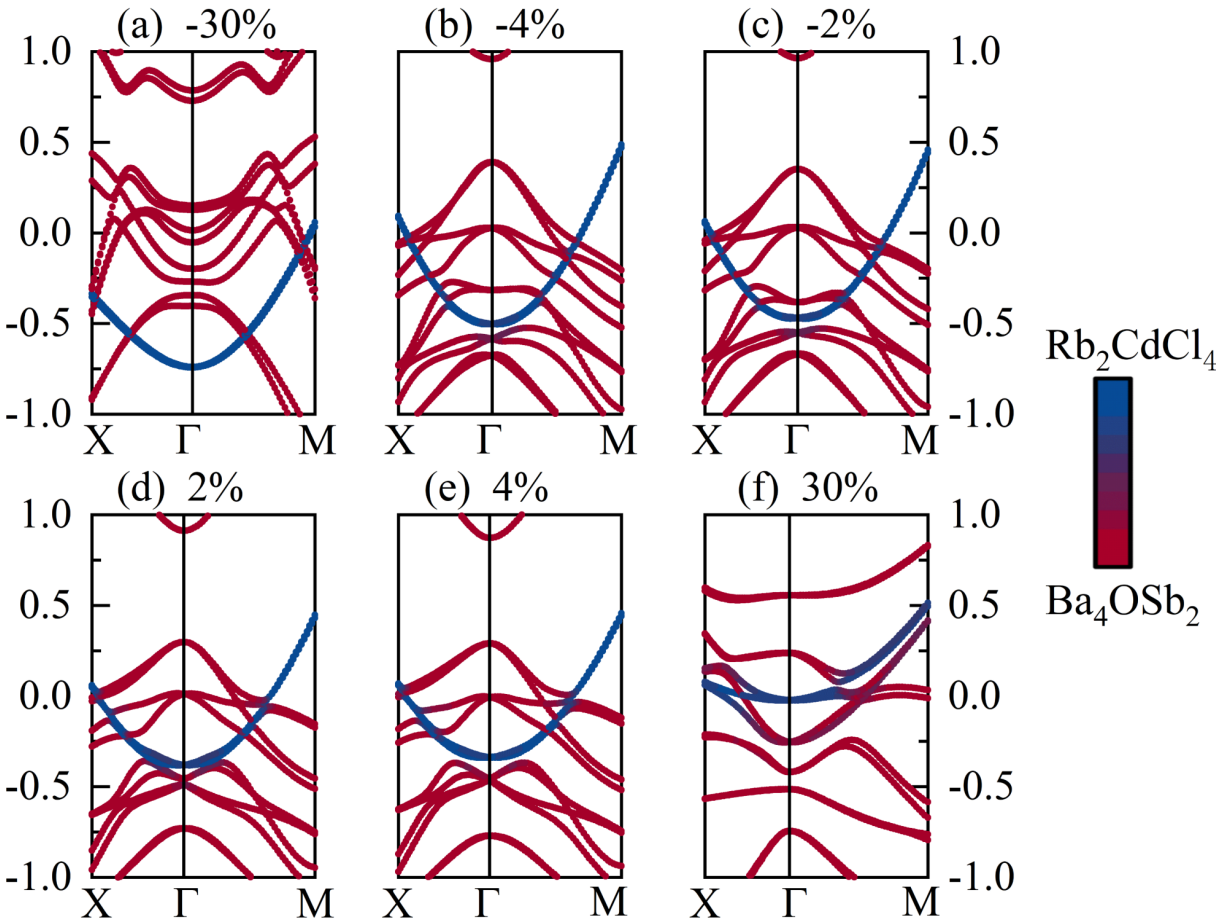

Figure S3 Projected band structures of Rb_2CdCl_4/Ba_4OSb_2 vdWH under various uniaxial strains at the PBE level with SOC.

When uniaxial and biaxial strains were applied, the type-III (broken-gap) band alignment is retained in Rb_2CdCl_4/Ba_4OSb_2 vdWH, which is different from the case of interlayer coupling. On the other hand, the compressive uniaxial and biaxial strains enlarge the tunneling window, while the tensile uniaxial and biaxial strains narrow the tunneling window. Therefore, the in-plane strain can retain the type-III band alignment and modulate the tunneling window.

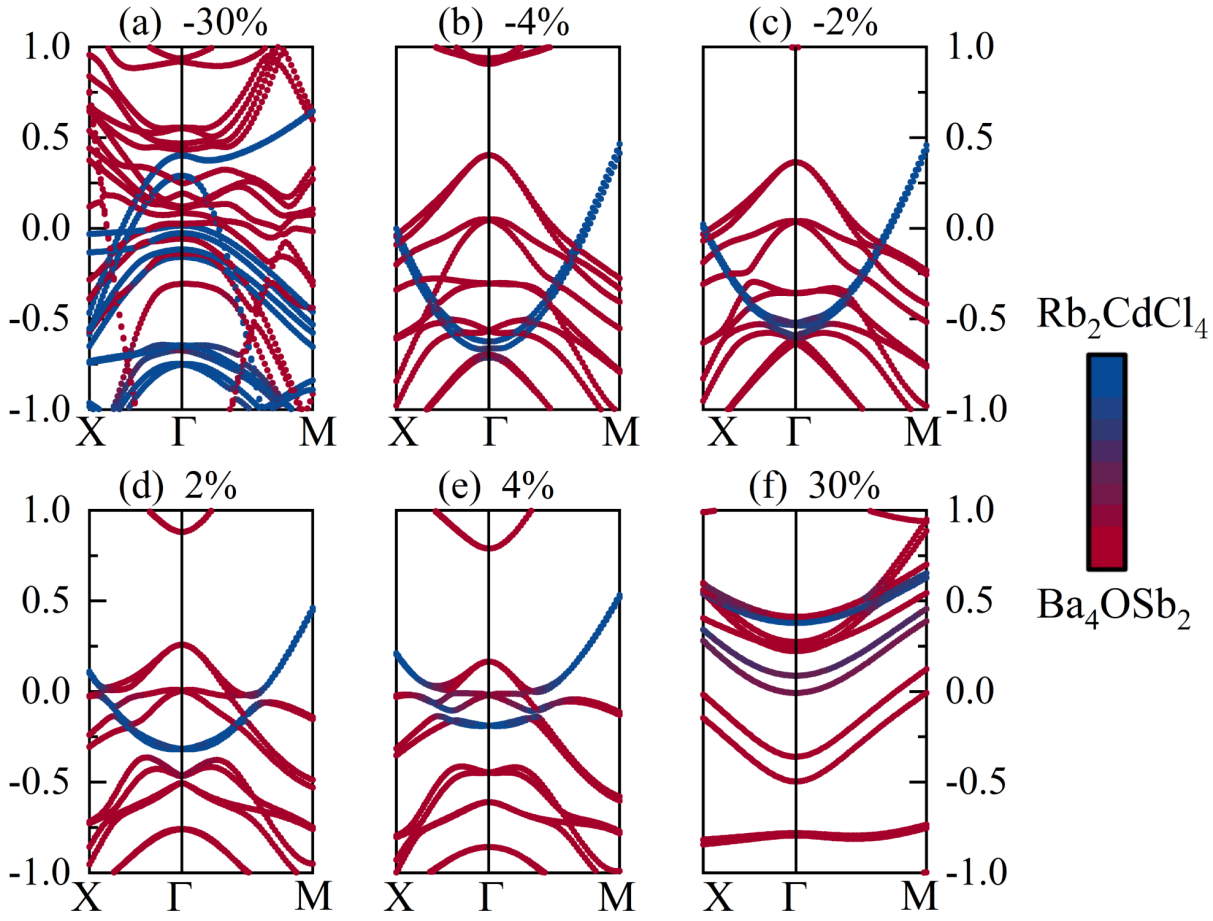

Figure S4 Projected band structures of Rb_2CdCl_4/Ba_4OSb_2 vdWH under various biaxial strains at the PBE level with SOC.

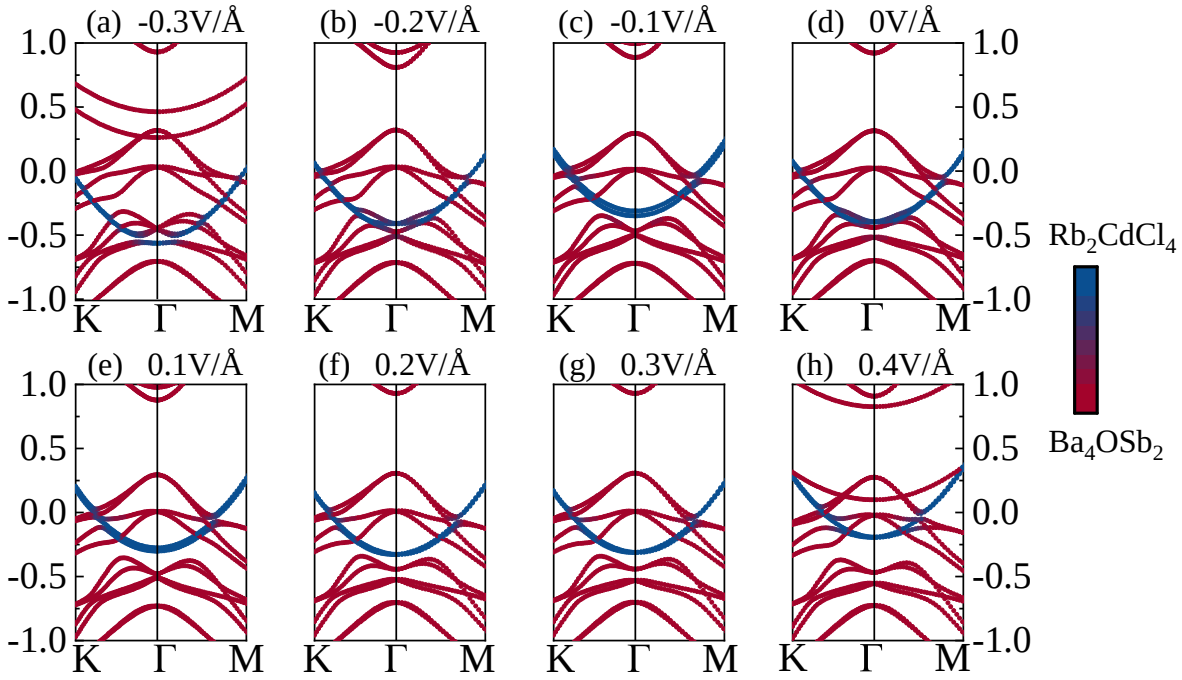

Figure S5 Projected band structures of Rb_2CdCl_4/Ba_4OSb_2 vdWH under various electric field at the PBE level with SOC.

Gate voltage is another way to effectively tune the electronic properties of multiple materials and devices. Thus, we wonder if an external electric field could trigger some interesting effects in the broken-gap Rb_2CdCl_4/Ba_4OSb_2 van de Waals heterostructure (vdWH). We calculate the electronic band structures of Rb_2CdCl_4/Ba_4OSb_2 vdWH under an external electric field applied along the z direction, pointing from the Ba_4OSb_2 layer toward the Rb_2CdCl_4 layer. Note that the direction of the negative electric field is the same as that of the built-in electric field. Fig. S5 shows the projected band structures and corresponding band alignments of Rb_2CdCl_4/Ba_4OSb_2 vdWH under several selected electric fields. It is found that the type-III (broken-gap) band alignment is retained in Rb_2CdCl_4/Ba_4OSb_2 vdWH under electric field. Moreover, the negative electric field enlarges the tunneling window, while the positive electric field narrows the tunneling window. When the strength of the negative electric field increases, the energy window is widened for tunneling, and thus the tunneling probability is increased. On the other hand, as the strength of the positive electric field increases, the energy window is narrow, and finally leading to type-II band alignment. This can be ascribed to the balance out between positive electric field and inner electric field. Therefore, the electric field can modify the tunneling window and realize multiple-band alignment transformation in 2D Rb_2CdCl_4/Ba_4OSb_2 vdWH.

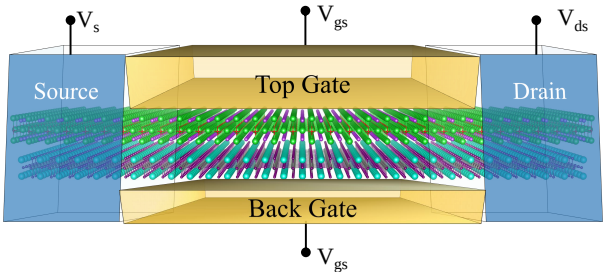

Figure S6 Schematic diagram of a multiple-purposed device based on Rb_2CdCl_4/Ba_4OSb_2 vdWH.

Finally, we propose a multiple-purposed device prototype based on Rb_2CdCl_4/Ba_4OSb_2 vdWH in Fig. S6. The device includes a source, a channel, a drain, and two gates. The source and drain provide the gate voltage driving carries, and the two gates can introduce the external electric field into the semiconducting channel. The device consisting of type-III band alignment of Rb_2CdCl_4/Ba_4OSb_2 vdWH is suitable for tunnel field-effect transistors, and the tunneling window can be adjusted by in-plane strain and electric field. When a tensile vertical strain is applied, the type-III band alignment is transformed to type-II band alignment, and the device can be used for unipolar electronic applications accordingly. Therefore, Rb_2CdCl_4/Ba_4OSb_2 vdWH is a promising candidate for future multifunctional devices.

References

[1] S. Siegel and E. Gebert, *Acta Cryst.*, 1964, **17**, 790–790.

[2] A. Kruglik, A. Vasilyev and K. Aleksandrov, *Phase Transit.*, 1989, **15**, 69–76.

[3] X. Li, S. Wang, S. Zhao, L. Li, Y. Li, B. Zhao, Y. Shen, Z. Wu, P. Shan and J. Luo, *Chem. Eur. J.*, 2018, **24**, 9243–9246.

[4] J. Li, Q. Yu, Y. He, C. C. Stoumpos, G. Niu, G. G. Trimarchi, H. Guo, G. Dong, D. Wang, L. Wang *et al.*, *J. Am. Chem. Soc.*, 2018, **140**, 11085–11090.

[5] J. Li, C. C. Stoumpos, G. G. Trimarchi, I. Chung, L. Mao, M. Chen, M. R. Wasielewski, L. Wang and M. G. Kanatzidis, *Chem. Mater.*, 2018, **30**, 4847–4856.

[6] B.-H. Chen and B. Eichhorn, *Mater. Res. Bull.*, 1991, **26**, 1035–1040.

[7] H. Limartha, B. Eisenmann, H. Schäfer and H. A. Graf, *Z. NATURFORSCH B.*, 1980, **35**, 1518–1524.

[8] C. Hadenfeldt and H.-U. Terschüren, *Z. Anorg. Allg. Chem.*, 1991, **597**, 69–78.

[9] S. Xia and S. Bobev, *J. Alloys Compd.*, 2007, **427**, 67–72.

[10] C. Hadenfeldt and H. Vollert, *JLCM.*, 1988, **144**, 143–151.

[11] M.-Y. Liao, Y.-C. Chiang, C.-H. Chen, W.-C. Chen and C.-C. Chueh, *ACS Appl. Mater. Interfaces*, 2020, **12**, 36398–36408.

[12] S. Hu, B. Xia, Y.-P. Lin, T. Katase, J. Fujioka, T. Kamiya, H. Hosono, K.-Z. Du and Z. Xiao, *Adv. Funct. Mater.*, 2020, **30**, 1909906.

[13] K. T. Butler, Y. Kumagai, F. Oba and A. Walsh, *J. Mater. Chem. C.*, 2016, **4**, 1149–1158.